European Commission
FP7, Grant Agreement 211743

Review of quantum non-demolition schemes for the Einstein Telescope

ET-010-09

Helge Müller-Ebhardt, Henning Rehbein, Stefan Hild, Andreas Freise, Yanbei Chen, Roman Schnabel, Karsten Danzmann and Harald Lück

Issue: 1

Date: September 18, 2009

Max-Planck-Institut für Gravitationsphysik (Albert-Einstein-Institut) and Universität Hannover, Callinstr. 38, 30167 Hannover, Germany
School of Physics and Astronomy, University of Birmingham, B15 2TT, UK
California Institute of Technology, M/C 130-33, Pasadena, California 91125

ET – Einstein gravitational wave Telescope – Design Study * A joint European Project
Web: http://www.et-gw.eu Email: EuropeanProjectsService@ego-gw.it

Contents

1 Introduction

In this note we want to discuss different "quantum non-demolition" (QND) [Bra1980, Bra1996, Bra1999] techniques, often also called quantum noise reduction methods, for the design study towards an European third-generation earth-bound laser interferometer gravitational-wave (GW) detector, the "Einstein Telescope" (ET) [ET]. The goal of this project is to provide a conceptual design of this detector having a hundred times better sensitivity than currently operating detectors (LIGO [Abb2004], VIRGO [Fio2002], GEO [Wil2002] and TAMA [And2001]). In the framework of the technical working group WP3, "Topology Identification", we shall on the one hand analyze the theoretically possible improvement in sensitivity produced by a certain QND technique for a detector of the envisaged scales and on the other hand we shall also comment on problems and disadvantages in the implementation of such techniques and their feasibility for the GW detection. We will review two main topologies [Fre2008]: the Michelson and the Sagnac interferometer. We will not provide the computational details but we will cite the relevant references. All the results had been obtained by using the travelling-waves approach in the framework of the two-photon formalism [Cav1985, Sch1985] with the approximation that the sideband frequencies are much smaller than the carrier laser frequency, as it is extensively reviewed in e.g. Ref. [Cor2005]. We will additionally use the fact that the considered sideband frequencies $\Omega/(2\pi) \sim 10\,\mathrm{Hz} - 10\,\mathrm{kHz}$ are in the same range as the interferometer's arm-cavity half-bandwidth γ and consequently, we will always use an approximation as it becomes suggested by the relation

$$T = 4\,\gamma\,L/c \sim \Omega\,L/c \ll 1\,, \tag{1}$$

which is Eq. (B7) of Ref. [Kim2001].

With different optical designs of the laser interferometer, it is possible to shape the spectral density of the arising quantum noise, which is the sum of radiation-pressure noise (dominating at low frequencies) and shot noise (dominating at high frequencies). Here the challenge is to lower the quantum noise in the required frequency band, which needs basically two inputs: *(i)* on the one hand the shape of the predicted classical (thermal) noise of the detector (manly investigated in WP2) and *(ii)* on the other hand the theoretically predicted GW forms which is the target of the observation (WP4). Then it is possible to compare different optical detector designs with respect to their sensitivity performance – optimizing over the relevant parameter space. Note that the classical noise depends on the optical design of the detector and that the different configurations will have different issues in their technical realizability. In this note we will make the simplification that *(i)* the classical noise of all the mirrors is uncorrelated and *(ii)* for each measured degree of freedom of each mirror (which

carrier laser frequency	$\omega_0/(2\pi)$	$c/(1064\,\mathrm{nm})$
sideband (or GW) frequency	$f = \Omega/(2\pi)$	$\sim 10\,\mathrm{Hz} - 10\,\mathrm{kHz}$
circulating optical power in the arm cavity	I_c	$3\,\mathrm{MW}$
mass of a single arm-cavity mirror	m	$120\,\mathrm{kg}$
arm-cavity length	L	$10\,\mathrm{km}$
characteristic frequency	$\iota_c^{1/3} = (\frac{8\,I_c\,\omega_0}{m\,L\,c})^{1/3}$	$\approx 2\pi\,80\,\mathrm{Hz}$
arm-cavity input mirror power-transmissivity	T	
arm-cavity half-bandwidth	$\gamma = T\,c/(4\,L)$	
homodyne detection angle	ζ	
sr-mirror amplitude-reflectivity	ρ	
sr-cavity length	l	
sr-cavity detuning phase	$\phi = [\omega_0\,l/c]_{\mathrm{mod}\,2\pi}$	
effective detuning for sr-Michelson	$\lambda = \gamma\,\frac{2\,\rho\,\sin 2\phi}{1+\rho^2+2\,\rho\,\cos 2\phi}$	
effective bandwidth for sr-Michelson	$\epsilon = \gamma\,\frac{1-\rho^2}{1+\rho^2+2\,\rho\,\cos 2\phi}$	
effective detuning for sr-Sagnac	$\lambda_1 = \gamma\,\frac{2\,\sqrt{\rho}\,\cos\phi}{1+\rho+2\sqrt{\rho}\,\sin\phi} = -\gamma^2\,\frac{\lambda_2}{\lambda_2^2+\epsilon_2^2}$	
effective bandwidth for sr-Sagnac	$\epsilon_1 = \gamma\,\frac{1-\rho}{1+\rho+2\sqrt{\rho}\,\sin\phi} = \gamma^2\,\frac{\epsilon_2}{\lambda_2^2+\epsilon_2^2}$	
input-squeezing factor in power	$e^{-2\,r}$	$10\,\mathrm{dB}$
angle of the input-squeezing ellipse	φ	

Table 1: Glossary of notations and some parameter values used for the calculations.

is subject to the carrier power) we assume 1/4 the classical motion of the classical noise of a dual-recycled Michelson interferometer with arm cavities.

There is an enormous effort in the GW community in order to increase the quality of the technical components of detectors further – such as the mirror and beam splitter materials, the suspension systems, the stability of the laser source, etc. – in order to decrease the amount of the classical noise. Already in the next generation of GW detectors, such classical noise sources will have taken a back seat at almost all frequencies. In order to reduce the classical noise floor even more, the idea is for future detectors to make use of cryogenic temperatures and to build them underground. In this note we will use a very optimistic estimation of the classical noise budget [Hil2008] so to say as the standard classical noise budget for ET. Here the seismic and the gravity gradient noise are assumed to be reduced by a huge amount due to the underground facility, the long suspension systems and gravity gradient noise subtraction. We assume that the suspension thermal noise can be reduced by a factor of 10 in amplitude compared to current estimations (with the simulation tool *Bench* [Bench]) for the Advanced LIGO detector [AdvLIGO] – while we assume the coating thermal noise to be reduce by a factor of 4.5, due to an increase in the laser beam size and due to the cooling of the mirrors. The complete classical noise budget is represented by the gray curves in e.g. Fig. 1: around 1 Hz at a level of $\sim 5\,10^{-21}\,/\sqrt{\mathrm{Hz}}$, while dropping to $\sim 10^{-24}\,/\sqrt{\mathrm{Hz}}$ at around 10 Hz. We will use the same key-parameter for the extent of the detector under investigation as in Ref. [Hil2008], such as an arm length of 10 km, mirror masses of 120 kg and a circulating optical power of 3 MW in the arm cavities (cf. Tab. 1). These parameter values are in the following analysis always fixed and not subject to any optimization process – even though they play a very important rule in the shape of the quantum noise, especially in the position of the peak sensitivity. But technical issues give some restrictions on these parameters. Even though the astrophysical target sources for the observation of a third generation GW detector may be totally different from those of the second generation, in this note we still optimize the sensitivity towards the detection of neutron star binary inspirals [Dam2000] in order to have a measure which is able to compare the different topologies. Note that this will be only the first step.

This note is organized as follows: in Sec. 2 we will start with reviewing the well-known behavior of the quantum noise arising in a simple Michelson interferometer with arm-cavities, as the example for a position meter. Observing the phase quadrature of the vacuum fields leaking out at the dark port of the interferometer, the

quantum noise spectral density is limited by the so-called standard quantum limit (SQL) [Bra1968, Bra1999] and therefore, the measurement is not QND. Mentioning the quantum noise in a simple Michelson in this note serves more as an introductory example. In Sec. 2.1 we shall review different modifications or extensions of the Michelson interferometer turning it into a QND device and will investigate the benefits and feasibility for the ET detector. The first candidate is detuned signal-recycling (SR) with a balanced homodyne detection, in addition with frequency-dependent input squeezing (Sec. 2.1.1) or with frequency-independent input squeezing and variational output (Sec. 2.1.2). For the sake of completeness we will shortly mention the local readout scheme (Sec. 2.1.3) and the double optical spring (Sec. 2.1.4). In Sec. 3 we will review the quantum noise properties of a speed meter, which can either be realized by a modification of the Michelson interferometer or by using a Sagnac topology. From the theoretical point of view, the quantum noise behavior in both schemes is equivalent. We will also apply the detuned SR technique (Sec. 3.1), in addition with frequency-dependent input squeezing (Sec. 3.1.1) or with frequency-independent input squeezing and variational output (Sec. 3.1.2). Then we will comment on a speed meter local readout scheme in Sec. 3.1.3. In Sec. 4 we will summarize our main conclusions and will venture to give some rating or recommendation.

2 Position meter: the Michelson interferometer

One could say that the Michelson interferometer is the standard design for a laser interferometer GW detector. It is well-investigated and there are a lot of experiences within the GW community of using Michelson interferometers. A simple Michelson interferometer can be equipped with different add-ons or tools in order to enhance the sensitivity. The power-recycling technique is already a standard tool which increases the optical power in the interferometer – or from another point of view lowers the necessary input power if a fixed circulating power is assumed (cf. Tab. 1). Using arm cavities also increases the optical power in the arms but moreover, it lowers the optical power which has to pass the beam splitter. This prevents thermal effects in the transmissive optics to become a major problem and also minimizes the bright port - dark port coupling due to the beam splitter motion [Har2004]. Since both techniques increase the circulating optical power in the arms they decrease the shot noise at high frequencies but at the same time they increase the radiation-pressure noise at low frequencies. In current detectors the radiation-pressure noise is no issue because it is covered by classical noise sources. The use of arm cavities raises the shot noise power spectral density at high frequencies [Kim2001] with $\sim f^2$ due to the finite cavity bandwidth (cf. Fig. 1) reducing the broadband feature of the detector's sensitivity. The quantum noise spectral density for a Michelson interferometer with arm cavities (optionally equipped with non-detuned SR), where the phase of the output fields is observed, is given in Eq. (27) of Ref. [Kim2001]. Here the radiation pressure noise power-spectral density reads

$$S_h^{\mathrm{rp}}(f) = \frac{1}{2}\,\frac{2\,\iota_c\,\gamma}{(2\pi\,f)^2\,(\gamma^2+(2\pi\,f)^2)}\;S_h^{\mathrm{SQL}}(f)\,, \tag{2}$$

while the shot noise power-spectral density reads

$$S_h^{\mathrm{shot}}(f) = \frac{1}{2}\,\frac{(2\pi\,f)^2\,\left(\gamma^2+(2\pi\,f)^2\right)}{2\,\iota_c\,\gamma}\;S_h^{\mathrm{SQL}}(f)\,. \tag{3}$$

Therefore, the quantum noise as the sum of radiation-pressure and shot noise is totally determined by only two parameters (cf. Tab. 1): *(i)* the characteristic frequency $\iota_c^{1/3}$ as defined in Eq. (20) of Ref. [Buo2003], which is equal to two times the circulating optical power divided by the carrier laser wavelength, the arm-cavity length and the reduced mirror mass; and *(ii)* the arm-cavity half-bandwidth γ, which is in the case of non-detuned SR replaced by the effective bandwidth ϵ. The quantum noise is limited by the strain-referred SQL, which is here given by

$$S_h^{\mathrm{SQL}}(f) = \frac{8\,\hbar}{m\,(2\pi\,f)^2\,L^2}\,. \tag{4}$$

The total quantum noise curve touches the SQL – and has therefore its peak sensitivity – at

$$f = f_q \equiv \frac{\gamma\,\sqrt{\sqrt{1+8\,\iota_c/\gamma^3}-1}}{2\,\sqrt{2}\,\pi} \overset{\iota_c \ll \gamma^3}{\approx} \frac{\sqrt{2\,\iota_c/\gamma}}{2\pi}\,. \tag{5}$$

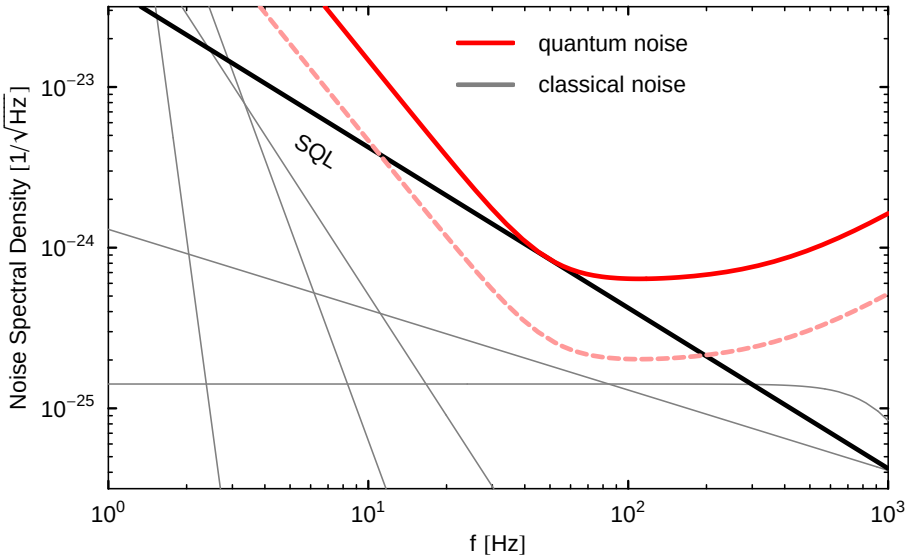

Figure 1: Example quantum noise spectral densities for a Michelson interferometer with arm cavities, having a half-bandwidth of $\gamma = 2\pi\,400\,\mathrm{Hz}$, and phase-quadrature readout. ET parameters from Tab. 1 as well as the standard noise budget are used. No input squeezing (solid curve) and with 10 dB frequency-dependent input squeezing (dashed curve). The gray curves represent the different classical noise contributions and the black line the SQL.

Increasing or decreasing the measurement frequency f_q at a fixed arm-cavity half-bandwidth simply shifts the quantum noise along the SQL-line (cf. Fig. 1). Increasing the arm-cavity half-bandwidth at a fixed measurement frequency makes the quantum noise curve more broadband, i.e. decreasing the quantum noise level simultaneously at high and at low frequencies. Due to the big gap between the assumed classical noise and the SQL a simple Michelson interferometer with the parameters as given in Tab. 1 would be totally dominated by the quantum noise (cf. Fig. 1) and therefore a waste of efforts in the classical noise reduction. For this scenario (cf. Fig. 1) we would have a lot of room to play with the shape of the quantum noise by applying different QND techniques.

Note that in a Michelson interferometer optical losses in the arm cavities are not a serious issue for the quantum noise when using currently available low-loss mirrors. In principle the power loss coefficient per round trip can be made as low as $T_{\mathrm{loss}} \approx 20\,10^{-6}$. Accurate to first order in the arm-cavity losses [Kim2001], the input field gets attenuated by $\mathcal{E} \leq 2\,T_{\mathrm{loss}}/T$ and the lost field gets replaced by coherent vacuum in the output at the interferometer's dark port while the phase shift that the interferometer cavities put onto the loss field is only half that put onto the dark-port input field. Furthermore, the radiation-pressure force acting onto the mirrors is increased by T_{loss}/T in power, which comes from the noise field. At the same time the signal becomes attenuated by $\mathcal{E}/2$ in power. This can be found in Eq. (101) of Ref. [Kim2001].

2.1 Detuned signal-recycling

The extensively theoretically [Buo2001, Buo2002, Buo2003] as well as experimentally [Fre2000, Som2005, Miy2006] investigated detuned SR technique allows to effectively manipulate the quantum noise. It was originally proposed by Meers in Ref. [Mee1988]: an additional mirror, the so-called SR mirror, is placed at the dark output port of the interferometer, reflecting parts of the signal modulation fields back into the interferometer and forming a SR cavity together with the input mirrors of the interferometer's arm cavities. The signal, which is the arm-cavity mirror's differential displacement, becomes recycled which means that it is basically amplified due to an increase in interaction time between the light and the mirrors. When the SR cavity is neither resonant nor anti-resonant with respect to the carrier frequency, the optical configuration is called detuned SR. Even though

the circulating optical power in the arm cavities of a Michelson interferometer with detuned SR is not modified, the optomechanical coupling induces an restoring force onto the differential motion of the arm-cavities mirrors, the optical spring effect [Buo2001], producing an additional resonance. The sensitivity is basically enhanced

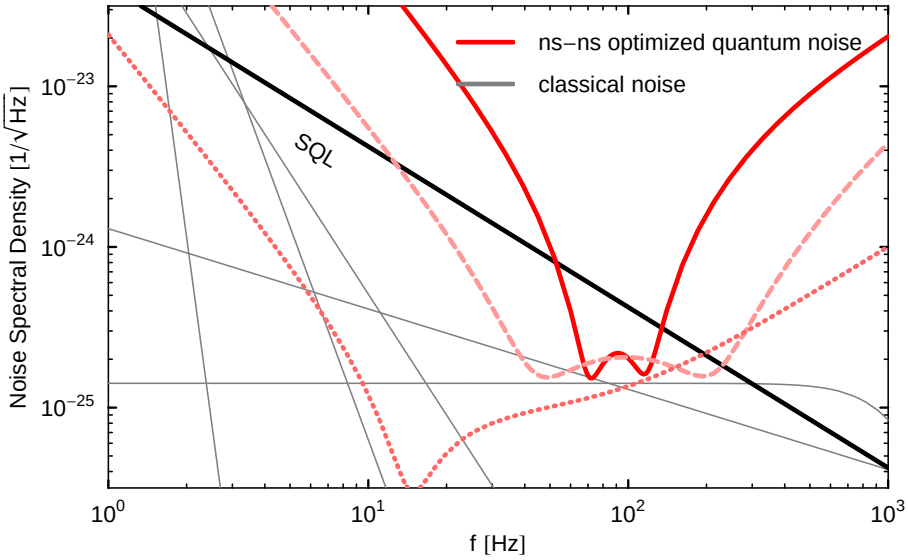

Figure 2: For neutron star binary inspirals optimized quantum noise spectral densities for a Michelson interferometer with arm cavities and detuned SR (solid curve) with an effective detuning of $\lambda = 2\pi\,136\,\mathrm{Hz}$, an effective half-bandwidth of $\epsilon = 2\pi\,8\,\mathrm{Hz}$ and a homodyne detection angle of $\zeta = 2\pi/3$. The dashed curve shows an optimization for 10 dB frequency-dependent squeezed input (effective detuning of $\lambda = 2\pi\,208\,\mathrm{Hz}$, effective half-bandwidth of $\epsilon = 2\pi\,60\,\mathrm{Hz}$ and homodyne detection angle of $\zeta = 0.44\,\pi$) and the dotted curve for variational output with 10 dB frequency-independent squeezed input (effective detuning of $\lambda = 2\pi\,4\,\mathrm{Hz}$, effective half-bandwidth of $\epsilon = 2\pi\,92\,\mathrm{Hz}$ and squeezing angle of $\varphi = 0$). ET parameters from Tab. 1 and the standard noise budget (gray curves) are used.

around the resonances, the optomechanical and the optical, but the price one has to pay is that sensitivity is lost especially at low frequencies.

Varying the SR parameters can differently shape the quantum noise curves (cf. solid curve in Fig. 2). Here only four parameters are important (cf. Tab. 1): again *(i)* the characteristic frequency $\iota_c^{1/3}$; *(ii)* the effective detuning λ (equal to the real part of the free optical resonance) and *(iii)* the effective half-bandwidth ϵ (equal to the imaginary part of the free optical resonance) which are both proportional to the arm-cavity half-bandwidth γ and further depend on the SR parameters, i.e. the reflectivity of the SR mirror and the detuning in the SR cavity, as defined in Eq. (18) of Ref. [Buo2003]; and *(iv)* the homodyne detection angle ζ. A full explicit expression for the quantum noise spectral density is given in Eq. (37) of Ref. [Buo2003]. At sideband frequencies significantly higher than the optical resonance frequency, the strain-referred quantum noise spectral density passes into its asymptote which is the same as for the non-detuned SR configuration and reads

$$S_h^{\mathrm{quant}}(f) \overset{f^2 \gg \lambda^2+\epsilon^2}{\longrightarrow} \frac{(2\pi\,f)^4}{4\,\iota_c\,\epsilon\,\cos^2\zeta}\,S_h^{\mathrm{SQL}}(f)\,, \tag{6}$$

i.e. the noise level at high frequencies drops with a higher characteristic frequency, a higher effective half-bandwidth and a homodyne detection close to the phase quadrature. At frequencies well-below the optomechanical resonance the asymptote is given by

$$S_h^{\mathrm{quant}}(f) \overset{f^2 \ll \lambda^2+\epsilon^2}{\longrightarrow} \frac{\iota_c}{4\,\epsilon\,(2\pi\,f)^2}\,\frac{\lambda^2+(2\,\epsilon-\lambda\,\tan\zeta)^2}{(\epsilon-\lambda\,\tan\zeta)^2}\,S_h^{\mathrm{SQL}}(f)\,. \tag{7}$$

The noise level at low frequencies is of course raised with a higher characteristic frequency but depends also on the effective half-bandwidth in combination with the effective detuning and the homodyne detection angle.

Around the resonances the structure of the quantum noise is much more complicated. Here the measurement frequency f_q not only shifts the quantum noise along the SQL-line but also modifies significantly the structure of the noise curve around the resonances. An optimization over the SR parameter space – i.e. varying, at a fixed characteristic frequency, the effective detuning, the effective half-bandwidth and the homodyne detection angle – towards the detection of neutron star binary inspirals gives the solid curve in Fig. 2. Due to the specifically fixed characteristic frequency, the specific wave-form of the signal and the shape of the classical noise, the optimal quantum noise is very narrow peaked around 100 Hz.

Note that also in a detuned signal-recycled Michelson interferometer optical losses in the arm cavities and in the SR cavity are not a serious issue [Buo2001]. The noise spectral density of a lossy SR interferometer can be found in Eq. (5.13) of Ref. [Buo2001].

2.1.1 Frequency-dependent squeezed input

Inserting optical squeezed (vacuum) states into the interferometer's dark port can enhance the quantum-noise-limited sensitivity of an interferometer [Cav1980]. The experimental generation of squeezed vacuum is today already readily available at high squeezing factors up to 10 dB [Vah2008] and down to sideband frequencies in the audio band [Vah2006]. Propagating the squeezing through two appropriately designed filter cavities, also called Kimble filters [Kim2001], first can reduce the total quantum noise spectral density by the squeezing factor [Har2003]. (For a detailed discussion about how to generally obtain the right Kimble filters see the Appendix A of Ref. [Pur2002].) But for a detuned signal-recycled interferometer, combining squeezed input and homodyne detection in this way [Har2003] is only sub-optimal [Buo2004]. (Note that a totally optimal combination of frequency-dependent input-squeezing and homodyne detection is unfortunately not realizable with Kimble filters as shown in Ref. [Buo2004].) Here the total quantum noise spectral density (as given in Eq. (37) of Ref. [Buo2003]) and therefore also Eq. (6)–(7), are just reduced by the squeezing factor. For the frequency-dependent squeezed input configuration, an optimization (again over the SR parameter space towards the detection of neutron star binary inspirals) gives the dashed curve in Fig. 2. The quantum noise curve of this configuration is still quite narrow peaked. Other SR parameter values of course allow a sensitivity curve which is slightly more broadband but then not anymore optimal for the detection of neutron star binary inspirals.

Optical losses in the filter cavities are quite important. The bandwidth of the filter cavities usually has to be of the same order as the arm-cavity bandwidth. Assuming then that the arm cavities already have the lowest loss one can in principle achieve, the filters have to be long – comparable long to the arm cavities is more than sufficient. From the technical point of view this assumption might not be actual anymore. If the filter cavities have lower loss, then they can be even built much smaller than the arm cavities. Here the losses in the filter cavities do actually not effect the signal part – only the quantum noise increases. More concrete, Eq. (42) of Ref. [Buo2004] shows that for low losses or long filter cavities, what approximately happens is that $(1-\mathcal{E})$ of the frequency-dependent squeezed input is replaced by coherent vacuum, where the loss factor $\mathcal{E}$ is frequency-dependent, but never exceeds the upper limit of sum over the filter cavity's ratio between end mirror and input mirror transmissivity (Eq. (47) of Ref. [Buo2004]). With 10 km long filters, even losses of 1000 ppm per filter do not significantly effect the quantum noise curve in Fig. 2.

An alternative to the frequency-dependent squeezed input technique is to use only one short filter cavity as a bandpass filter with two squeezed inputs and an additional homodyne detection [Cor2004, Kha2008, Kha2009]. This method can also reduce the total quantum noise spectral density by the squeezing factor and is even less suspectable to losses in the filter cavity.

2.1.2 Variational output and frequency-independent squeezed input

For another (sub-optimal) configuration it was suggested in Ref. [Buo2004] that frequency-independent squeezed vacuum states are inserted into the dark port of a detuned signal-recycled interferometer and the output is sent through two Kimble filters after leaking out of the interferometer but before the homodyne detection is

performed. A very simple expression of the resulting quantum noise spectral density is given in Eq. (76) of Ref. [Buo2004]. Here we obtain at high frequencies similar to Eq. (6) that

$$S_h^{\rm quant}(f) \longrightarrow e^{-2\,r}\,\frac{(2\pi\,f)^4}{4\,\iota_c\,\epsilon\,\cos^2\varphi}\,S_h^{\rm SQL}(f)\,, \tag{8}$$

where $e^{-2\,r}$ is the squeezing factor and φ is the frequency-independent squeezing angle. While at low frequencies we obtain (for $\lambda \neq 0$ – since otherwise in the non-detuned case, the quantum noise spectral density becomes equal to a constant at low frequencies, i.e. $S_h^{\rm quant} \to 2\,\hbar\,\gamma/(L^2\,m\,\iota_c\,\cos^2\zeta)$)

$$S_h^{\rm quant}(f) \longrightarrow e^{-2\,r}\,\frac{\lambda^2\,\iota_c}{4\,\epsilon\,(2\pi\,f)^2\,(\lambda\,\sin\varphi+\epsilon\,\cos\varphi)^2}\,S_h^{\rm SQL}(f)\,. \tag{9}$$

The noise level at low frequencies has a totally different dependence on the effective half-bandwidth, the effective detuning and the squeezing angle than in Eq. (7). An optimization over the SR parameter space – now varying, at a fixed characteristic frequency, the effective detuning, the effective half-bandwidth and the squeezing angle – towards neutron star binary inspirals gives the dotted curve in Fig. 2. The optimal parameters are very close to a non-detuned configuration. Due to the very low classical noise budget, this configuration can increase the sensitivity towards the detection of neutron star binary inspirals much more compared to the other sub-optimal configuration and it results also in a much broader sensitivity curve. Especially at low frequencies this configuration can improve the sensitivity a lot.

Here optical losses in the filter cavities are a very important factor – at low frequencies they are even disastrous. When optical losses are significant and when the radiation-pressure noise is strong, the variational readout becomes less effective, because in such a case, it is required to bring enough of the amplitude quadrature in order to cancel the radiation-pressure noise and this also introduces significantly higher noise (of the order of $\mathcal{E}$) due to optical losses. Moreover, optical losses remove $\mathcal{E}$ of the at low frequencies already weak signal (which lies in the phase quadrature) from the output. The signal of the radiation-pressure noise cancelling variational output scheme drops namely as $\sim f^2$ in amplitude. Even if the filters are comparable long to the arm cavities, i.e. 10 km, a small loss, e.g. 100 ppm, can already completely remove the positive effect of the variational output at low frequencies. This transforms the dotted curve in Fig. 2 into a curve similar to the dashed curve in Fig. 1.

2.1.3 Local readout scheme

The local readout configuration [Reh2007] severs mainly as a low cost add-on for second generation interferometers, as Advanced LIGO [AdvLIGO], which make use of the detuned SR technique but for which the input-squeezing technique is not available. An additional local meter uses the optical bar effect [Bra1997] in the signal-recycled interferometer at low frequencies which usually weakens the sensitivity of the interferometer with a conventional readout. This can be considered as a practical and direct incorporation of the optical bar detection scheme [Bra1997] (or even optical lever detection scheme [Kha2002a]) into currently planned second-generation interferometers. In fact, the so-called central Michelson degree of freedom, which is sensed by the local meter, is in the current detectors already measured to keep the signal-extraction port of the interferometer in dark fringe. However, the sensitivity of the current Michelson control signal must be improved dramatically in order to be turned into the desired regime [Reh2007]. But for a third generation detector this technique may be not enough to enhance the quantum-noise-limited sensitivity (cf. Fig. 3).

The combination with squeezed input is tricky – we need to obtain the optimal configuration if both interferometers have frequency-dependent input squeezing or variational output. In Fig. 3 the dashed curve represents a local readout scheme where only the local meter has 10 dB frequency-dependent input-squeezing with the same parameters as for the solid curve – the configuration is yet not optimized.

2.1.4 Double optical spring

The double optical spring configuration [Reh2008] is mainly intended to remove the instability which is introduced by a single optical spring. A proof of principle has already been demonstrated in a table-top experi-

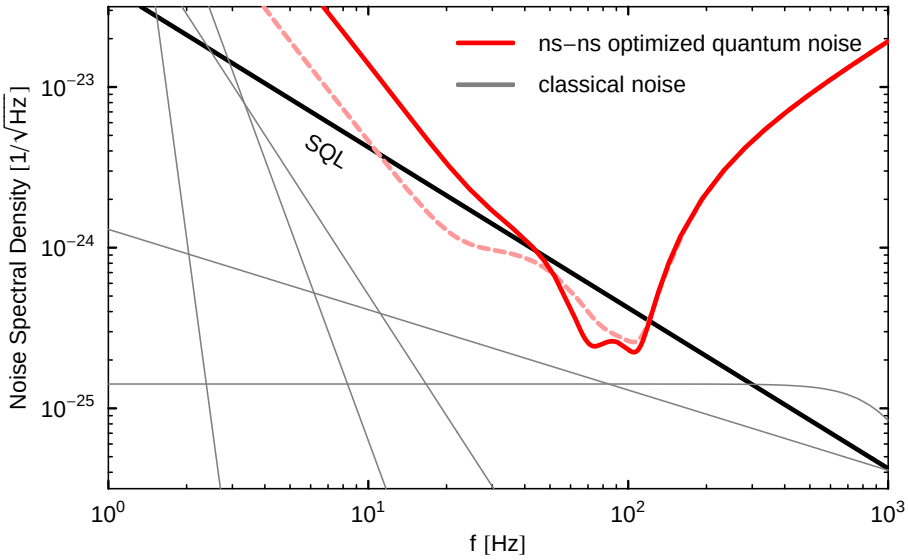

Figure 3: For neutron star binary inspirals optimized quantum noise spectral densities for a local readout scheme (solid curve). The dashed curve shows 10 dB frequency-dependent squeezed input for the local meter. For the large-scale interferometer ET parameters from Tab. 1 and an effective detuning of $\lambda = 2\pi\,128\,\mathrm{Hz}$, an effective half-bandwidth of $\lambda = 2\pi\,4\,\mathrm{Hz}$ and a homodyne detection angle of $\zeta = 0.22\,\pi$ are used. The local meter has 1 kW optical power after the beam splitter, a bandwidth of 200 Hz and a homodyne detection angle of $0.04\,\pi$. As usual the standard noise budget (gray curves) is used.

ment [Cor2007]. It does not degenerate the sensitivity of a GW detector if the outputs are filtered and combined appropriately – it can even improve the sensitivity of a second-generation GW detector [Reh2008]. However, using this technique will definitely be not enough for third-generation detectors – especially on such optimistic classical noise estimations as we use here.

3 Speed meter: the Sagnac interferometer

The idea of constructing an optical speed meter was to measure the difference in position within a certain time which is at first order proportional to the speed and by doing so to totally avoid the quantum back action of the measurement, i.e. the radiation-pressure noise. But this can unfortunately not be totally realized [Kha2002b]. The specific feature of a speed meter is that at low frequencies, the quantum noise becomes parallel to the SQL, roughly up to the arm-cavity half-bandwidth and can even be significantly below – the quantum noise power level is at low frequencies approximately proportional to the cube of arm-cavity half-bandwidth over characteristic frequency, i.e. $\sim \gamma^3/\iota_c$, times the SQL. Whereas at high frequencies the quantum noise power spectral density follows $\sim f^4/(\gamma\,\iota_c)$.

There exist different proposed designs on how to realize a speed meter interferometer: to turn a Michelson interferometer into a speed meter by adding a sloshing cavity [Pur2002, Pur2002] or by using polarizing optics [Dan2004, McK2008]; building a Sagnac interferometer with triangular ring cavities [Che2003] or special quadratic ring cavities [Mue2005] in the arms. But as shown in Ref. [Che2003], the quantum noise in a Sagnac interferometer with ring cavities in the arms and non-detuned SR is equal to the quantum noise in a Michelson interferometer with a sloshing cavity – ignoring the influence of optical losses. The biggest problem is probably that there is no experimental experiences in using an optical speed meter as a GW detector.

In the following we will stick to analyzing the Sagnac interferometer with ring cavities in the arms. The quantum noise spectral density can be found in Eq. (22) and a short discussion about technical issues in Sec. IV of Ref. [Che2003]. It turns out that in a Sagnac interferometer optical losses in the arm cavities are at low

frequencies a serious issue due to the low signal. The optical losses can quite easily destroy the speed meter effect at low frequencies. The signal in a Sagnac interferometer drops below the bandwidth towards low frequencies with $\sim f$ in amplitude. This low signal could also be a technical problem. Furthermore, the special noise couplings in a Sagnac interferometer have to be analyzed [Che2009].

3.1 Detuned signal-recycling

The signal-recycled Sagnac interferometer has two optical resonances due to the two coupled resonators – but no optomechanical resonance. The optomechanical coupling modifies the dynamical reduced mass of the mirrors,

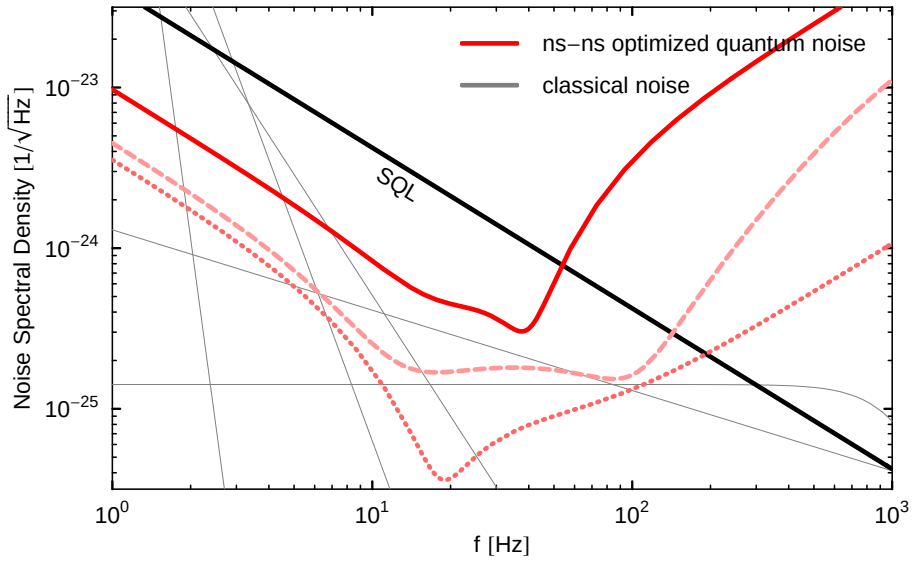

Figure 4: For neutron star binary inspirals optimized quantum noise spectral densities for a Sagnac interferometer with arm cavities and detuned SR (solid curve) with an arm-cavity half-bandwidth of $\gamma = 2\pi\,50\,\mathrm{Hz}$, an effective detuning of $\lambda_1 = 2\pi\,42\,\mathrm{Hz}$, an effective half-bandwidth of $\epsilon_1 = 2\pi\,30\,\mathrm{Hz}$ and a homodyne detection angle of $\zeta = 0.475\,\pi$. The dashed curve shows an optimization for 10 dB frequency-dependent squeezed input (arm-cavity half-bandwidth of $\gamma = 2\pi\,75\,\mathrm{Hz}$, effective detuning of $\lambda_1 = 2\pi\,95\,\mathrm{Hz}$, effective half-bandwidth of $\epsilon_1 = 2\pi\,54\,\mathrm{Hz}$ and homodyne detection angle of $\zeta = 0.475\,\pi$) and the dotted curve for variational output with 10 dB frequency-independent squeezed input (arm-cavity half-bandwidth of $\gamma = 2\pi\,25\,\mathrm{Hz}$, effective detuning of $\lambda_1 = 2\pi\,0.5\,\mathrm{Hz}$, effective half-bandwidth of $\epsilon_1 = 2\pi\,8.6\,\mathrm{Hz}$ and squeezing angle of $\varphi = 0$). ET parameters from Tab. 1 and the standard noise budget (gray curves) are used.

adding an optical inertia [Mue2005]. Here five parameters are responsible for the shape of the quantum noise spectral density: again *(i)* the characteristic frequency $\iota_c^{1/3}$; *(ii)* the arm-cavity half-bandwidth γ; *(iii)* the real part of one of the optical resonances λ_1 and *(iv)* the imaginary part of one of the optical resonances ϵ_1 which are both proportional to the arm-cavity bandwidth and further depend on the SR parameters, i.e. reflectivity of the SR mirror and detuning of the SR cavity, as defined in Eq. (2.21) of Ref. [Mue2009]; and *(v)* the homodyne detection angle ζ. The quantum noise spectral density can be computed from Eq. (2.45) of Ref. [Mue2009]. At high frequencies the quantum noise spectral density reads similar to the Michelson case (c.f. Eq. (6))

$$S_h^{\mathrm{quant}}(f) \longrightarrow \frac{(2\pi\,f)^4}{4\,\iota_c\,(\epsilon_1+\epsilon_2)\,\cos^2\zeta}\,S_h^{\mathrm{SQL}}(f)\,, \tag{10}$$

while at low frequencies it is parallel to the SQL and given by

$$S_h^{\rm quant}(f) \;\rightarrow\; \left(1+\left(\frac{2\,\iota_c\,(\epsilon_1+\epsilon_2)\,(\epsilon_1\epsilon_2-\lambda_1\lambda_2)^2}{(\epsilon_1^2+\lambda_1^2)(\epsilon_2^2+\lambda_2^2)((\epsilon_1^2+\lambda_1^2)(\epsilon_2^2+\lambda_2^2)-\iota_c(\lambda_1+\lambda_2))}-\tan\zeta\right)^2\right)\times \frac{\left((\epsilon_1^2+\lambda_1^2)(\epsilon_2^2+\lambda_2^2)-\iota_c\,(\lambda_1+\lambda_2)\right)^2}{4\,\iota_c\,(\epsilon_1+\epsilon_2)\,(\epsilon_1\epsilon_2-\lambda_1\lambda_2)^2}\;S_h^{\rm SQL}(f)\,, \tag{11}$$

where $\lambda_1 > 0$ and $\lambda_2 < 0$ are the real parts of the optical resonances and $\epsilon_{1,2}$ the corresponding imaginary parts. The two optical resonances are not independent and their relation is given in Tab. 1 or in Eq. (2.22) of Ref. [Mue2009]. In the case of a resonant SR cavity this relation simplifies to

$$\lambda_1 = -\lambda_2 = \gamma\,\sqrt{1-\mu^2}\,, \quad \epsilon_1 = \epsilon_2 = \gamma\,\mu\,, \tag{12}$$

where $0 < \mu = (1-\rho)/(1+\rho) < 1$ with the SR mirror reflectivity ρ. In the anti-resonant SR case we find

$$\lambda_1 = \lambda_2 = 0\,, \quad \epsilon_1 = \epsilon_2 = \gamma\,\left(\mu-\sqrt{\mu^2-1}\right)\,, \tag{13}$$

where this time $1 < \mu = (1+\rho)/(1-\rho)$.

We can see from Eq. (10)–(11) that there is not an universal homodyne detection angles which minimizes the quantum noise at same time at high and at low frequencies: cancelling radiation pressure noise at low frequencies is usually at the expense of sensitivity at high frequencies. It has turned out that the optimal choice for the detection of neutron star binary inspirals is, however, a very weakly detuned SR, nearly resonant. The optimal quantum noise curve is then typical for a speed meter, i.e. parallel to the SQL up to the arm-cavity half-bandwidth (cf. solid line in Fig. 4). In principle the detuned SR can help to broaden the sensitivity curve in the mid-frequency regime and opening it a little more to the high frequencies.

3.1.1 Frequency-dependent squeezed input

The most sensitive configuration for neutron star binary inspirals of a signal-recycled Sagnac interferometer with frequency-dependent squeezed input produces – by using a more detuned SR cavity – a much broader quantum noise curve (cf. dashed curve in Fig. 4).

The optical losses in the filter cavities are here much less crucial than the losses in the arm cavities. As in the Michelson interferometer with frequency-dependent squeezed input, filters comparable long to the arm cavities can even bear losses of 1000 ppm.

3.1.2 Variational output and frequency-independent squeezed input

The quantum noise spectral density for a variational output and frequency-independent squeezed input and signal-recycled Sagnac interferometer reads at high frequencies (similar to Eq. (10))

$$S_h^{\rm quant}(f) \longrightarrow e^{-2\,r}\;\frac{(2\pi\,f)^4}{4\,\iota_c\,(\epsilon_1+\epsilon_2)\,\cos^2\varphi}\;S_h^{\rm SQL}(f)\,, \tag{14}$$

while at low frequencies it is given by

$$S_h^{\rm quant}(f) \rightarrow e^{-2\,r}\;\frac{\left(\iota_c\,(\lambda_1+\lambda_2)-\left(\epsilon_1^2+\lambda_1^2\right)\,\left(\epsilon_2^2+\lambda_2^2\right)\right)^2}{4\,\iota_c\,(\epsilon_1+\epsilon_2)\,(\epsilon_1\,\epsilon_2-\lambda_1\,\lambda_2)^2\,\cos^2\varphi}\;S_h^{\rm SQL}(f)\,. \tag{15}$$

We can see from Eq. (14)–(15) that at both, high and low frequencies, the phase quadrature of the vacuum input has to be squeezed, i.e. $\varphi = 0$. Then the variational output and frequency-independent squeezed input

method can increase the sensitivity at low frequencies even more (cf. dotted curve in Fig. 4) compared to the simple single-recycled Sagnac interferometer. Preferably, the SR cavity is here nearly anti-resonant. In the non-detuned situation, i.e. with a resonant ($0 < \mu < 1$) or anti-resonant ($\mu > 1$) SR cavity, the quantum noise spectral density of a signal-recycled Sagnac interferometer with variational output is quite easy to modulate: at low frequencies equal to $\gamma^3/(8\,\iota_c\,\mu)$ times squeezing times the SQL; at its (more or less peaked (small μ) or flat (high μ) minimum) (at $\Omega = \gamma$) equal to $\gamma\,\mu/2$ times squeezing times the SQL; and at high frequencies equal to $(2\pi\,f)^4/(8\,\iota_c\,\gamma\,\mu)$ times squeezing times the SQL. Decreasing the arm-cavity half-bandwidth is therefore good for the sensitivity in the low- and the mid-frequency regime while bad at high frequencies and also moves the peak sensitivity towards low frequencies. Increasing μ is good at low and high frequencies while bad in the mid-frequency regime. In this non-detuned case, increasing the characteristic frequency is always good.

Again optical losses in the filter cavities are additionally to the arm cavity losses an crucial factor.

3.1.3 Local readout scheme

Our investigation suggests that adding a local meter to a speed meter can probably not increase the sensitivity further even though a detuned signal-recycled speed meter has interesting transducer properties [Mue2005]. This is because the speed meter is already very sensitive at low frequencies.

4 Conclusion

In this note we have worked out that if a third-generation GW detector *(i)* is equipped with notedly heavier mirrors (here of about 120 kg) and with a circulating optical power limited by 3 MW in the arm cavities (cf. Tab. 1) and *(ii)* establishing a classical noise floor which is as low as assumed in this note (cf. e.g. Fig. 1), the quantum noise of a Michelson interferometer with arm cavities and detuned SR (as used for the Advanced LIGO detector design) will be the limiting factor of the sensitivity over all frequencies in the detection band. Optimizing the sensitivity e.g. towards the detection of inspiraling neutron star binaries, the quantum noise of such a detector becomes too narrowband peaked, which throws away a huge amount of sensitivity at high and low frequencies. This is very inappropriate for a third-generation GW detector whose astrophysical target sources are not restricted to neutron star binaries and which should therefore be a rather broadband device. One possible way out of this problem is to use squeezed optical (vacuum) states – which is already an experimentally well investigated tool – together with long filter cavities – which is experimentally not yet well enough investigated – in order to broaden the sensitivity simultaneously at low and at high frequencies. Furthermore, we have found that the add-ons for the Advanced LIGO detector, the local readout scheme and the double optical spring configuration, are as a stand-alone tool not able to reduce the quantum noise in a adequate way. Note that the local readout scheme also includes the class of optical bar detector schemes. A very promising alternative – in terms of quantum noise – is to use speed meter configurations, which already cancel the back-action noise at low frequencies and can also be combined with input-squeezing techniques. But these configurations still need to be rigorously analyzed in terms of the (specific) noise couplings and call for an experimental verification.

References

[Bra1980] V. B. Braginsky, Y. I. Vorontsov, and K. S. Thorne, *Quantum nondemolition measurements*, Science **209**, 547 (1980). 1

[Bra1996] V. B. Braginsky and F. Y. Khalili, *Quantum nondemolition measurements: the route from toys to tools*, Rev. Mod. Phys. **68**, 1 (1996). 1

[Bra1999] V. B. Braginsky and F. Y. Khalili, *Quantum measurement*, Cambridge University Press (1999). 1, 3

[ET] *Einstein Telescope*, http://www.et-gw.eu/. 1

[Abb2004] B. Abbott et al., *Detector description and performance for the first coincidence observations between LIGO and GEO*, Nucl. Inst. and Meth. A **517**, 154 (2004). 1

[Fio2002] L. D. Fiore and *the VIRGO collaboration*, *The present status of the VIRGO Central Interferometer*, Class. Quant. Grav. **19**, 1421 (2002). 1

[Wil2002] B. Willke et al., *The GEO 600 gravitational wave detector*, Class. Quantum Grav. **19**, 1377 (2002). 1

[And2001] M. Ando and the TAMA collaboration, *Stable Operation of a 300-m Laser Interferometer with Sufficient Sensitivity to Detect Gravitational-Wave Events within Our Galaxy*, Phys. Rev. Lett. **86**, 3950 (2001). 1

[Fre2008] A. Freise, S. Chelkowski, S. Hild, W. Del Pozzo, A. Perreca, and A. Vecchio, *Triple Michelson Interferometer for a Third-Generation Gravitational Wave Detector*, http://arxiv.org/abs/0804.1036 (2008). 1

[Cav1985] C. M. Caves and B. L. Schumaker, *New formalism for two-photon quantum optics*, Phys. Rev. A **31**, 3068 (1985). 1

[Sch1985] B. L. Schumaker and C. M. Caves, *New formalism for two-photon quantum optics*, Phys. Rev. A **31**, 3093 (1985). 1

[Cor2005] T. Corbitt, Y. Chen, and N. Mavalvala, *Mathematical framework for simulation of quantum fields in complex interferometers using the two-photon formalism*, Phys. Rev. A **72**, 013818 (2005). 1

[Kim2001] H. J. Kimble, Y. Levin, A. B. Matsko, K. S. Thorne, and S. P. Vyatchanin, *Conversion of conventional gravitational-wave interferometers into quantum nondemolition interferometers by modifying their input and/or output optics*, Phys. Rev. D **65**, 022002 (2001). 1, 3, 4, 6

[Hil2008] S. Hild, S. Chelkowski, and A. Freise, *Pushing towards the ET sensitivity using conventional technology*, http://arxiv.org/abs/0810.0604 (2008). 2

[Bench] http://www.ligo.mit.edu/bench/bench.html (v. 4.0). 2

[AdvLIGO] *Advanced LIGO reference design*, http://www.ligo.caltech.edu/docs/M/M060056-07/M060056-07.pdf (2007). 2, 7

[Dam2000] T. Damour, B. R. Iyer, and B. S. Sathyaprakash, *Frequency-domain P-approximant filters for time-truncated inspiral gravitational wave signals from compact binaries*, Phys. Rev. D **62**, 084036 (2000). 2

[Har2004] J. Harms, R. Schnabel, and K. Danzmann, *Finite mass beam splitter in high power interferometers*, Phys. Rev. D **70**, 102001 (2004). 3

[Buo2003] A. Buonanno and Y. Chen, *Scaling law in signal recycled laser-interferometer gravitational-wave detectors*, Phys. Rev. D **67**, 062002 (2003). 3, 4, 5, 6

[Bra1968] V. B. Braginsky, *Classical and quantum restrictions on detection of weak distributions of a macroscopic oscillator*, Sov. Phys. JETP **26**, 831 (1968). 3

[Buo2001] A. Buonanno and Y. Chen, *Quantum noise in second generation, signal-recycled laser interferometric gravitational-wave detectors*, Phys. Rev. D **64**, 042006 (2001). 4, 5, 6

[Buo2002] A. Buonanno and Y. Chen, *Signal recycled laser-interferometer gravitational-wave detectors as optical springs*, Phys. Rev. D **65**, 042001 (2002). 4

[Fre2000] A. Freise, G. Heinzel, K. A. Strain, J. Mizuno, K. D. Skeldon, H. Lueck, B. Willke, R. Schilling, A. Ruediger, W. Winkler, *Demonstration of detuned dual recycling at the Garching 30m laser interferometer*, Phys. Lett. A **277**, 135 (2000). 4

[Som2005] K. Somiya, P. Beyersdorf, K. Arai, S. Sato, S. Kawamura, O. Miyakawa, F. Kawazoe, S. Sakata, A. Sekido, and N. Mio, *Development of a frequency-detuned interferometer as a prototype experiment for next-generation gravitational-wave detectors*, Appl. Opt. **44**, 3179 (2005). 4

[Miy2006] O. Miyakawa, R. Ward, R. Adhikari, M. Evans, B. Abbott, R. Bork, D. Busby, J. Heefner, A. Ivanov, M. Smith, R. Taylor, S. Vass, A. Weinstein, M. Varvella, S. Kawamura, F. Kawazoe, S. Sakata, and C. Mow-Lowry, *Measurement of optical response of a detuned resonant sideband extraction gravitational wave detector*, Phys. Rev. D **74**, 022001 (2006). 4

[Mee1988] B. J. Meers, *Recycling in laser-interferometric gravitational-wave detectors*, Phys. Rev. D **38**, 2317 (1988). 4

[Cav1980] C. M. Caves, *Quantum-mechanical noise in an interferometer*, Phys. Rev. D **23**, 1693 (1980). 6

[Vah2008] H. Vahlbruch, M. Mehmet, S. Chelkowski, B. Hage, A. Franzen, N. Latstzka, S. Gossler, K. Danzmann, and R. Schnabel, *Observation of Squeezed Light with 10 dB Quantum-Noise Reduction*, Phys. Rev. Lett. **100**, 033602 (2008). 6

[Vah2006] H. Vahlbruch, S. Chelkowski, B. Hage, A. Franzen, K. Danzmann, and R. Schnabel, *Coherent Control of Vacuum Squeezing in the Gravitational-Wave Detection Band*, Phys. Rev. Lett. **97**, 011101 (2006). 6

[Pur2002] P. Purdue and Y. Chen, *Practical speed meter designs for quantum nondemolition gravitational-wave interferometers*, Phys. Rev. D **66**, 122004 (2002). 6, 8

[Har2003] J. Harms, Y. Chen, S. Chelkowski, A. Franzen, H. Vahlbruch, K. Danzmann, and R. Schnabel, *Squeezed-input, optical-spring, signal-recycled gravitational-wave detectors*, Phys. Rev. D **68**, 042001 (2003). 6

[Buo2004] A. Buonanno and Y. Chen, *Improving the sensitivity to gravitational-wave sources by modifying the input-output optics of advanced interferometers*, Phys. Rev. D **69**, 102004 (2004). 6, 7

[Cor2004] T. Corbitt, N. Mavalvala, and S. E. Whitcomb, *Optical cavities as amplitude filters for squeezed fields*, Phys. Rev. D **70**, 022002 (2004). 6

[Kha2008] F. Y. Khalili, *Increasing future gravitational-wave detectors sensitivity by means of amplitude filter cavities and quantum entanglement*, Phys. Rev. D **77**, 062003 (2008). 6

[Kha2009] F. Khalili, H. Miao, and Y. Chen, *Increasing the sensitivity of future gravitational-wave detectors with double squeezed-input*, in preparation (2009). 6

[Reh2007] H. Rehbein, H. Mueller-Ebhardt, K. Somiya, C. Li, R. Schnabel, K. Danzmann, and Y. Chen, *Local readout enhancement for detuned signal-recycling interferometers*, Phys. Rev. D **76**, 062002 (2007). 7

[Bra1997] V. B. Braginsky, M. L. Gorodetsky, and F. Y. Khalili, *Optical bars in gravitational wave antennas*, Phys. Lett. A **232**, 340 (1997). 7

[Kha2002a] F. Y. Khalili, *The 'optical lever' intracavity readout scheme for gravitational-wave antennae*, Phys. Lett. A **298**, 308 (2002). 7

[Reh2008] H. Rehbein, H. Mueller-Ebhardt, K. Somiya, S. L. Danilishin, R. Schnabel, K. Danzmann, and Y. Chen, *Double optical spring enhancement for gravitational wave detectors*, Phys. Rev. D **78**, 062003 (2008). 7, 8

[Cor2007] T. Corbitt, Y. Chen, E. Innerhofer, H. Mueller-Ebhardt, D. Ottaway, H. Rehbein, D. Sigg, S. Whitcomb, C. Wipf, and N. Mavalvala, *An all-optical trap for a gram-scale mirror*, Phys. Rev. Lett. **98**, 150802 (2007). 8

[Kha2002b] F. Y. Khalili, *Quantum speedmeter and laser interferometric gravitational-wave antennae*, http://arxiv.org/abs/gr-qc/0211088 (2002b). 8

[Pur2002] P. Purdue, *Analysis of a quantum nondemolition speed-meter interferometer*, Phys. Rev. D **66**, 022001 (2002). 8

[Dan2004] S. L. Danilishin, *Sensitivity limitations in optical speed meter topology of gravitational-wave antennas*, Phys. Rev. D **69**, 102003 (2004). 8

[McK2008] K. McKenzie, private communication (2008). 8

[Che2003] Y. Chen, *Sagnac interferometer as a speed-meter-type, quantum-nondemolition gravitational-wave detector*, Phys. Rev. D **67**, 122004 (2003). 8

[Mue2005] H. Mueller-Ebhardt, K. Somiya, R. Schnabel, K. Danzmann, and Y. Chen, *Signal-recycled Sagnac interferometer*, unpublished manuscript (2005). 8, 9, 11

[Che2009] S. Chelkowski, *A Topology Review: The Sagnac Effect*, https://workarea.et-gw.eu/et/WG3-Topology/document_dir/0901meetinghannover/chelkowski-the_sagnac_effect.ppt. 9

[Mue2009] H. Mueller-Ebhardt, Ph.D. thesis, *On quantum effects in the dynamics of macroscopic test masses*, Leibniz Universitaet Hannover, http://www.aei.mpg.de/hannover-de/77-files/dissertationen/PhDThesis_MuellerEb.pdf (2009). 9, 10